

# Finding strong lenses in CFHTLS using convolutional neural networks

C. Jacobs<sup>1</sup>★, K. Glazebrook<sup>1</sup>, T. Collett<sup>2</sup>, A. More<sup>3</sup>, C. McCarthy<sup>4</sup>

<sup>1</sup>*Centre for Astrophysics and Supercomputing, Swinburne University of Technology, P.O. Box 218, Hawthorn, VIC 3122, Australia*

<sup>2</sup>*Institute of Cosmology and Gravitation, University of Portsmouth, Burnaby Rd, Portsmouth, PO1 3FX, UK*

<sup>3</sup>*Kavli IPMU (WPI), UTIAS, The University of Tokyo, Kashiwa, Chiba 277-8583, Japan*

<sup>4</sup>*School of Software and Electrical Engineering, Swinburne University of Technology, P.O. Box 218, Hawthorn, VIC 3122, Australia*

## ABSTRACT

We train and apply convolutional neural networks, a machine learning technique developed to learn from and classify image data, to Canada-France-Hawaii Telescope Legacy Survey (CFHTLS) imaging for the identification of potential strong lensing systems. An ensemble of four convolutional neural networks was trained on images of simulated galaxy-galaxy lenses. The training sets consisted of a total of 62,406 simulated lenses and 64,673 non-lens negative examples generated with two different methodologies. The networks were able to learn the features of simulated lenses with accuracy of up to 99.8% and a purity and completeness of 94–100% on a test set of 2000 simulations. An ensemble of trained networks was applied to all of the 171 square degrees of the CFHTLS wide field image data, identifying 18,861 candidates including 63 known and 139 other potential lens candidates. A second search of 1.4 million early type galaxies selected from the survey catalog as potential deflectors, identified 2,465 candidates including 117 previously known lens candidates, 29 confirmed lenses/high-quality lens candidates, 266 novel probable or potential lenses and 2097 candidates we classify as false positives. For the catalog-based search we estimate a completeness of 21–28% with respect to detectable lenses and a purity of 15%, with a false-positive rate of 1 in 671 images tested. We predict a human astronomer reviewing candidates produced by the system would identify ~20 probable lenses and 100 possible lenses per hour in a sample selected by the robot. Convolutional neural networks are therefore a promising tool for use in the search for lenses in current and forthcoming surveys such as the Dark Energy Survey and the Large Synoptic Survey Telescope.

**Key words:** gravitational lensing: strong – methods: statistical

## 1 INTRODUCTION

Gravitational lensing is a consequence of the relativistic curvature of spacetime by massive objects such as galaxies, groups and galaxy clusters (Einstein 1936; Zwicky 1937). Lensing phenomena can tell us much about the characteristics of distant objects and about the universe itself across cosmic time (Wambsganss 1998; Blandford & Narayan 1992; see Treu & Ellis 2015 for an overview). So-called strong lensing occurs where the gravitational potential of a lensing body is sufficient, and the position of a distant source is aligned such that multiple images of the source are produced and are detectable (Schneider et al. 2006; Treu 2010). Since the discovery of the first strongly-lensed quasar by Walsh et al. (1979), the search for and study of strong lenses has become an increasingly active field of astronomy. Strong lenses have numerous scientific uses including constraining the mass content and density profiles of galaxies, both dark matter and baryons (Treu

& Koopmans 2002; Bradač et al. 2002; Treu & Koopmans 2004; Sonnenfeld et al. 2015; Oguri et al. 2014; Auger et al. 2010; Collett et al. 2017) and allowing us to study otherwise undetectable young galaxies at high redshift when magnified by these gravitational telescopes (e.g. Newton et al. 2011; Quider et al. 2009; Zheng et al. 2012). Strong lenses are valuable for cosmology research, allowing us to constrain cosmological parameters such as the Hubble constant and dark energy equation of state, especially when time delay information is present such as in the case of lensed quasars (Refsdal 1964; Tewes et al. 2013; Suyu et al. 2013; Oguri et al. 2012; Collett & Auger 2014; Bonvin et al. 2016).

Only several hundred high-quality examples of galaxy-galaxy strong lenses are known (Collett 2015, the Masterlens database<sup>1</sup>), but current and next-generation wide surveys are likely to capture many more. Oguri & Marshall (2010) predict some 8000 lensed

★ E-mail: colinjacobs@swin.edu.au

<sup>1</sup> Database of confirmed and probable lenses from all sources, curated by the University of Utah. <http://admin.masterlens.org>

quasars are to be found in Large Synoptic Survey Telescope (LSST) (Ivezic et al. 2008) imaging and of order 1000 in the Dark Energy Survey (The DES Collaboration 2005) (DES)<sup>2</sup>. Treu (2010) predicts  $\sim 1$  lens per square degree with ground-based telescopes and Collett (2015) performed modelling suggesting  $\sim 2400$  galaxy-galaxy strong lenses should be identifiable in DES given an optimal stacking strategy, and of order  $10^5$  should be detectable in the LSST and Euclid (Amiaux et al. 2012) survey databases.

Lenses are scientifically rich; the trick is discovering them. Identifying strong lenses from amongst the many millions of non-lensing galaxies in the surveys of the next decade presents an interesting challenge. Lenses can be complex, spanning a range of morphologies, sizes and colours. Describing them, whether in code or for a human audience, is difficult to do without ambiguity.

With survey databases now in the terabyte-petabyte range, visual search of each potential lens galaxy by a human astronomer is no longer a feasible option, and so we need algorithms to find candidates for us. Previous automation strategies have included searching for features characteristic of strong lenses such as arcs and rings (Lenzen et al. 2004; Alard 2006; Estrada et al. 2007; Seidel & Bartelmann 2007; More et al. 2012; Gavazzi et al. 2014), fitting geometric parameters measuring an arc shape and searching for blue residuals in galaxy-subtracted images.

Marshall et al. (2009) and Brault & Gavazzi (2015) modeled potential lens galaxies candidate as a strong lens system and used the model's fit to the data as an estimate lens candidate likelihood.

Other approaches include using principal component analysis to subtract galaxies from imaging data (Joseph et al. 2014); parameterising the colour and shape of lensed quasars (Chan et al. 2015); and training thousands of citizen scientists on simulated images and then having them visually inspect cutouts (Marshall et al. 2016; More et al. 2016, hereafter SWI and II). }

Each methodology has successfully identified tens to hundreds of new lenses or high-quality candidates for follow-up (e.g. 59 in SWII). The problem faced by any automated strategy is the wide variety of morphologies present in strong lens systems and the potential for confusion with non-lenses, such as blue spiral galaxies. The difficulty in parameterising the full range of potential lenses has meant that inspection by human experts has remained both a cornerstone and bottleneck in lens-finding efforts.

In contrast to traditional approaches, machine learning classification techniques forego human intuitions regarding the weighting and relationships of significant features of the dataset and instead algorithmically extract a useful parameterisation from patterns present in the data only (see Jordan & Mitchell (2015) for a brief overview of current machine learning applications). The application of machine learning techniques to 'big data' challenges in astronomy is an active field of research at present. Artificial Neural Networks (ANNs) in particular have been successfully applied to astronomical problems. Dieleman et al. (2015) used convolutional neural networks to replicate human judgements about Sloan Digital Sky Survey (SDSS) galaxy morphology as part of a GalaxyZoo Kaggle challenge<sup>3</sup> and Huertas-Company et al. (2015) applied them to morphological classification in the CANDELS fields. Hoyle (2016) used deep learning (see Section 2) techniques for photometric redshift estimation. Schawinski et al. (2017) employed Generative Adversarial networks (Goodfellow et al. 2014) to develop a novel deconvolution technique and recover features

in SDSS galaxy images. In the lens-finding arena, Bom et al. (2017) employed neural networks and the Mediatrix Filamentation Method, while Ostrovski et al. (2017) applied Gaussian Mixture Models to the lensed quasar search.

The success of these machine learning techniques in other areas of astronomy, and more broadly in computer vision, makes them a promising candidate for learning and detecting the particular morphology of strong lenses. However, inherent in all supervised learning methodologies, and convolutional neural networks in particular, is the need for a large, diverse and fully-labelled training set with which to tune the network's weights. Training sets for complex image classification networks are typically of the order of  $10^6$  images and anything smaller than  $10^4$  images is unlikely to suffice for robust training of a complex network which may have order  $10^7$  to  $10^9$  parameters to be optimized. The work is further complicated by the rarity of strong lensing systems, with the implication that any sub-optimal classifier will swamp good potential lenses with false positives.

In this work we develop the application of convolutional neural networks to detecting the morphology of galaxy-galaxy lenses in optical images. We focus in particular on developing a synthetic training set of sufficient size and quality, and on ensuring that false positives were minimised. We use the lens quality grade scale as outlined in SWII, with images 0) unlikely to contain a lens, 1) possibly containing a lens, 2) probably containing a lens and 3) almost certainly containing a lens. In this paper we define false positives as any candidates that we judge to be below grade 1.

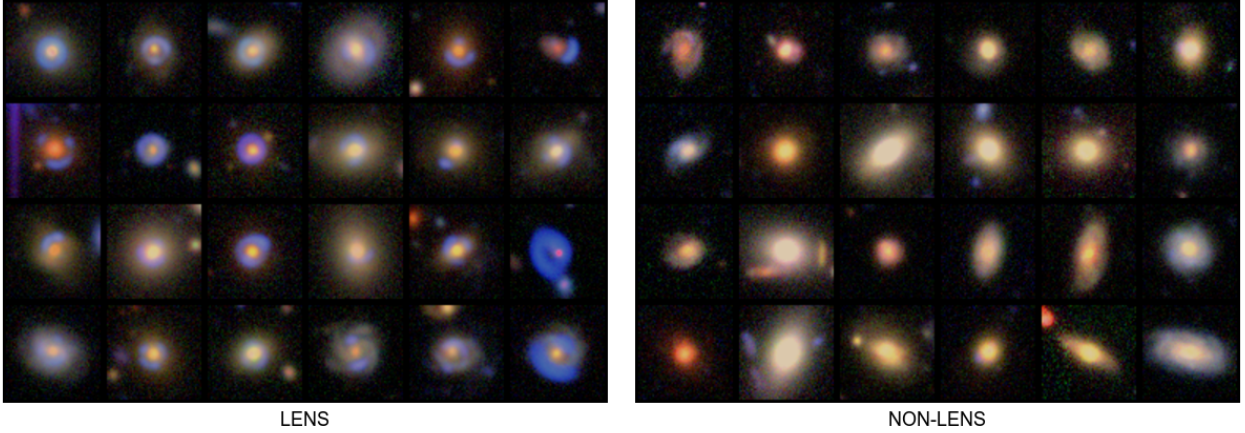
The Canada France Hawaii Telescope Legacy Survey (CFHTLS) was chosen for our search as it has been extensively searched for strong lenses previously, providing us with an opportunity to benchmark the performance of this approach. As well as visual searches (Elyiv et al. (2013), Sygnet et al. (2010)) and serendipitous discoveries (Thanjavur 2009) there have been several previous robotic searches of the entire survey as part of the CFHTLS Strong Lensing Legacy Survey (SL2S) (Cabanac et al. 2007). More et al. (2012) used the ARCFINDER robot and Gavazzi et al. (2014) used the RINGFINDER algorithm to detect galaxy and cluster-scale strong lenses. These two searches, in addition the SPACEWARPS search, have collectively identified over 500 lenses and potential lenses which we can use to assess the effectiveness of our own algorithm. These searches and the lenses they discovered are detailed in Section 2.2.

In this paper we present our convolutional neural network-based lens finder and apply it to the CFHTLS survey. The paper is organised as follows: Section 2 provides a brief overview of artificial neural networks and the training process that powers them, and details the results of previous automated lens searches in the survey. In Section 3 we describe the challenges of lens finding and how we assemble our networks and the simulated lens training sets to train them, as well as the two strategies we employ in their application to the survey data. In Section 4 we apply our lens finder to 171 degrees of the CFHTLS survey and describe the lens candidates we recover, including known, confirmed lenses and novel candidates. In Section 5 we examine the limitations of the two survey search approaches, the use of ensembles of neural networks, and how best to quantify the performance of the robot. Finally, in Section 6 we summarise the performance of our lens finder and provide a brief outlook of how future work may improve its performance and usefulness to astronomy.

<sup>2</sup> <http://www.darkenergysurvey.org>

<sup>3</sup> <https://www.kaggle.com/c/galaxy-zoo-the-galaxy-challenge>

## Training set 1 (SIMCT)



## Training set 2 (LensPop)

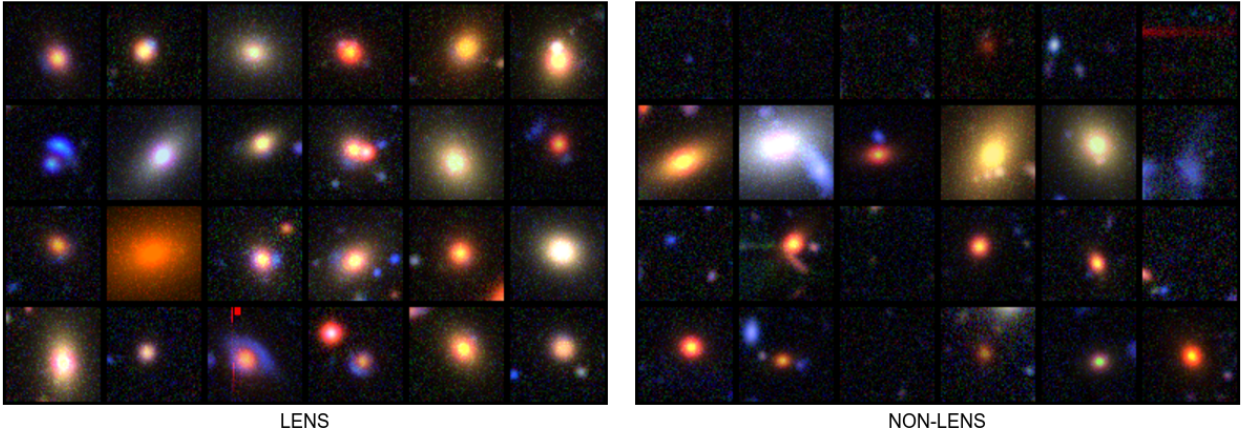


**Figure 1.** Example synthetic lens images from two training sets. Top: synthetic lensed sources on real survey galaxies. Bottom: Synthetic source and deflector, on real survey backgrounds.

## 2 BACKGROUND

Artificial Neural Networks (ANNs) were first described as far back as the 1950s or before (Rosenblatt 1957) and were refined over decades, but fell into relative disuse in favour of other algorithms due to performance and scaling issues. More recent advances in the algorithms, including improved network initialisation (Hinton & Salakhutdinov 2006), optimized gradient descent methods (Duchi et al. 2011; Zeiler 2012), dropout (Hinton et al. 2012), as well as improvements in hardware and the availability of large labelled data sets, have enabled “deep learning” - training ANNs with many layers - and a resurgence in their use. In recent years the field of computer vision has been revolutionized by advancements in deep learning techniques, in particular the use of convolutional neural networks (Fukushima 1980; Lecun et al. 1998). (“ConvNets”). In 2012 Krizhevsky et al. (2012), employing a convolutional neural network of novel design, entered the benchmark

ImageNet Large-Scale Visual Recognition Challenge<sup>4</sup> (ILSVRC) (Russakovsky et al. 2015) and were able to surpass in accuracy the state-of-the-art of conventional computer vision techniques by 10%, an impressive margin. Since then the development and application of convolutional neural networks remains an active area of research (Zeiler & Fergus 2014; Szegedy et al. 2014; Simonyan & Zisserman 2014; He et al. 2015).

Artificial neural networks, named by analogy to the neuronal network in the brain that inspired their design, are constructed as a layered network of interconnected nodes (“neurons”), each of which takes a weighted vector as inputs and outputs a scalar value passed through an activation function - a differentiable function that introduces non-linearity into the network. At the first layer, the raw inputs are weighted and passed as inputs to a layer of input neurons. This is repeated for an arbitrary number of intermediate “hidden” layers. At the last layer, the outputs are interpreted as an approx-

<sup>4</sup> An annual competition considered the benchmark in computer vision performance, with a training set of  $10^6$  images across 1000 categories. <http://www.image-net.org/challenges/LSVRC/>



imation function appropriate to the problem domain, such as the probability that the input is member of a particular class. For a network of sufficient size and complexity, arbitrary logic can be represented in the connections between artificial neurons, encapsulated by the weights that parameterise the network.

Convolutional neural networks extend ANNs by taking advantage of the spatial relationship between input values, namely, the pixels in an image. In a convolution layer, instead of fully connecting all neurons, groups of input neurons are applied to small regions of neighbouring pixels, and the associated weights are shared amongst many groups. This approach has several desirable properties. It vastly reduces the number of weights that characterise the network, and exploits key characteristics of the visual domain such as the spatial significance of neighbouring pixels and translational invariance. These small groups of weights (kernels) are convolved with the image and act as feature detectors. At earlier layers they perform the function of detecting simple geometric features such as edges or patches of colour; at later levels the hierarchy of features becomes increasingly abstract. A network may first activate on curves and corners; then features that resemble wheels and doors; and finally recognise the arrangement of these features as a truck.

In assessing the quality of a sample produced by a network, the astronomical terminology of purity and completeness differ in their definitions slightly from the terms used in the computer science literature (see Table 3 and Table 7).

## 2.1 Training Neural Networks

The essence of machine learning techniques is the algorithmic extraction of patterns from data. Supervised learning techniques, such as that presented here, take a labelled (i.e. pre-classified) data set and use it to iteratively optimize a function that parameterizes the differences between the classes of data presented. The training of ANNs involves the optimization of a loss function using the techniques of backpropagation (Hecht-Nielsen 1989) and stochastic gradient descent (Bottou 2010). In brief: Mathematically we consider our neural network as a large differentiable function that is parameterized by a set of weights  $\mathbf{W}$  which, for any input vector  $\mathbf{x}$ , outputs a vector  $\mathbf{y} \in \mathbb{R}^N$  which we interpret as the probabilities that  $\mathbf{x}$  is a member of a defined set of  $N$  categories:

$$\mathbf{y} = F(\mathbf{x}, \mathbf{W}) \quad (1)$$

We then take a training set  $\hat{\mathbf{X}}$  consisting of  $k$  examples, together with labels of known correct categories  $\hat{\mathbf{y}}$ . We define a loss function  $L$  such that:

$$L = L(\mathbf{y}, \hat{\mathbf{y}}) \text{ where } \hat{\mathbf{y}} = F(\hat{\mathbf{X}}, \mathbf{W}) \quad (2)$$

such that  $L \approx 0$  if  $\mathbf{y} = \hat{\mathbf{y}}$ , i.e. all examples classified correctly with probability 1 and  $L$  increases as  $\mathbf{y}$  and  $\hat{\mathbf{y}}$  diverge, i.e. the number of mis-classifications on the training set increases. For instance: a cross entropy loss function per Cao et al. (2007). The problem then becomes to minimize the function  $L$  by finding the optimum set of weights  $\mathbf{W}$  given our training set  $\hat{\mathbf{X}}$ . We do this using a gradient descent method, iteratively calculating the gradients  $\frac{\partial L}{\partial W_i}$  for each  $\mathbf{x}$  in  $\hat{\mathbf{X}}$  and  $W_i$  in  $\mathbf{W}$ , updating  $\mathbf{W}$  accordingly until we converge to a minimum value of  $L$ . The back-propagation algorithm for calculating the weight gradients and the stochastic gradient descent method used to minimize  $L$  and converge on a set of weights are described fully in LeCun et al. (1989).

**Table 1.** The lenses and potential lenses within the CFHTLS survey reported in previous searches which we use as a benchmark to measure lens-finder performance. Those with reported spectroscopic or imaging follow-up (as compiled by the Masterlens database) we consider confirmed.

Source	Candidates	Confirmed
SL2S More+12	117	57
SL2S Sonnenfeld+13	13	13
SL2S Gavazzi+14	376	34
More+15	59	0
Total	565	104

## 2.2 Known lenses and candidates

Previous systematic searches of the CFHTLS data have yielded over 500 potential lens candidates. The CFHTLS Strong Lensing Legacy Survey (SL2S) (Cabanac et al. 2007; More et al. 2012; Gavazzi et al. 2014; Sonnenfeld et al. 2013) employed several methods to identify strong lenses in the CFHTLS imaging. More et al. (2012) used the ArcFinder (Seidel & Bartelmann 2007) algorithm, visually inspecting 1000 candidates per square degree, and yielding a final sample of 127 high-quality candidates. From Sonnenfeld et al. (2013) we include 13 further SL2S lenses confirmed with spectroscopic follow-up. Gavazzi et al. (2014), using the RingFinder robot, report a purity and completeness of 42% and 29% (86% and 25% after visual inspection) on simulations, and present 330 good quality (grade > 2) candidates from visual inspection of a sample of 2500 (13%) returned by the algorithm on CFHTLS imaging data. In addition, we include 55 candidates listed from earlier versions of RingFinder and other searches that were not included in the other papers. Of these SL2S candidates, 104 have follow-up indicating definite or probable lens status.

We also include 59 new candidates identified in SWII of grades 1-3, as discovered by 37,000 citizen scientists of the SPACEWARPS program. These lenses form a test set we use for optimising search parameters.

We found 13 other confirmed lenses lying within the CFHTLS footprint had been discovered serendipitously in Hubble Space Telescope (HST) images, and two in SDSS spectroscopic data. These lenses are not detectable in CFHTLS images and so we do not include them in the analysis.

Table 1 depicts the catalog we assembled after removing duplicates and several lenses for which we did not have imaging available.

## 3 METHOD

Constructing our lens-finding robot and using it to identify candidates in the survey involves the following steps. Firstly, we construct several training sets of simulated lenses and non-lenses. We also assemble a test set of real survey images containing the 59 SWII lenses/candidates. We use the simulated images to train two convolutional neural networks of our own design using an open source deep learning framework, and evaluate their performance on the test set. Counting the number of lenses recovered and the false positives identified in the test set allows us to optimise several parameters for use in a wider search of the entire survey image dataset (“all-survey search”). We then evaluate  $6.4 \times 10^8$  60x60 postage stamps from the CFHTLS survey with each of the two trained networks to produce a candidate set for grading by visual inspection. Subsequently, we adjust the training set and network architecture

**Table 2.** Details of the four Convnets applied to the search. ConvNet1 and ConvNet2 were trained for the all-survey search, then two networks with an extra convolutional layer and training sets tailored for the catalog-based search were trained. All four networks were applied to the catalog-based search.

Network	Training set	Architecture	Ensemble
ConvNet1	TS 1	ARCH1	All-survey, catalog
ConvNet2	TS 2	ARCH1	All-survey, catalog
ConvNet3	TS 3	ARCH2	Catalog
ConvNet4	TS 4	ARCH2	Catalog

and train two further neural networks, and use an ensemble of all four of our networks in a more restricted, catalog-based search of potential lensing galaxies. The networks, training sets and architectures used are summarised in Table 2.

### 3.1 Training Data

In order to apply convolutional neural networks to the lens-finding problem, we must first assemble a training set to optimise the network. The number of known galaxy-galaxy strong lenses is of order  $10^2$ , which practice suggests is several orders of magnitude below the minimum required to usefully train a ConvNet. Furthermore, images of known lenses stem from a heterogeneous mix of surveys, instruments and bands. We must employ an alternate strategy to assemble a training set of sufficient size and consistency. Fortunately, gravitational lensing can be readily modelled using basic physical principles. Here we take the approach of generating synthetic data - simulated lenses in sufficient quantity to form a practical training set.

We assume that, if the artificial lenses are of sufficient quality, then the network will learn lensing features, such as colour and geometry, sufficiently well to generalize successfully to real astronomical data. Conversely, any errors or biases in the training set are likely to be reflected in the ConvNet’s performance, not necessarily in predictable ways. For lens finding, we require that the lensing galaxies and sources should match the colour, size and shape distributions of the real universe as closely as possible; the training set should be adapted for the seeing and filters of the particular target survey, in this case CFHTLS; noise (shot and sky) should match the realistic values for the integration times present in the survey imaging.

Free parameters include the number of examples, the format and dimensions of each training image, the location of lenses in the images and the composition of the negative examples (i.e. non-lens training images).

We employ two strategies to assemble training images conforming to the above constraints. The first strategy involves identifying potential deflector galaxies in the survey, and adding a simulated lensed source galaxy to the survey image. This method is implemented in the SIMCT<sup>5</sup> described in detail in SWII but can be summarized as follows. Potential deflector galaxies, primarily large, massive early-type galaxies (ETGs), are selected from the CFHTLS catalog by brightness, colour and photometric redshift. A model mass distribution is assigned to each galaxy using a singular isothermal ellipsoid profile and aligned with the image. Artificial sources are constructed according to the observed parameters

of redshift, luminosity and size and given plausible surface brightness profiles and ellipticities. The multiple images of the source are then generated and added to the deflector image using GRAVLENS (Keeton 2001) raytracing code with noise and seeing simulated to match those present in the CFHTLS. As the number of synthetic lens examples is limited to the lens candidate catalog, the data is augmented by applying three 90 degree rotations and a random translation of  $\pm 10$  pixels in each axis to create four training images per catalog galaxy.

Our second strategy for generating a training set is to generate mock images where both the lens and source are simulated. This has the advantage that the number of examples that can be generated is effectively infinite, but has the disadvantage that noise, seeing and artifacts must also be simulated to well match real survey data. We do this using a modified version of the LENSPOP<sup>6</sup> code (Collett 2015). LENSPOP uses the observed velocity dispersion function of elliptical galaxies (Choi et al. 2007) to generate a population of singular isothermal ellipsoid (SIE) lenses, with realistic mass, redshift and ellipticity distributions. Lens light is then added using the fundamental plane relation (Hyde & Bernardi 2009) assuming a de Vaucouleurs Profile and the spectral energy distribution of an old, passive galaxy. Sources are assumed to have an elliptical exponential profile, with redshifts, sizes and colours drawn from the simulated faint source catalogue of Connolly et al. (2010).

In principle LENSPOP can simulate lenses with extremely faint arcs or extremely small Einstein Radii. In practice such systems are undetectable as lenses and will not contain sufficiently strong features to usefully train the ConvNets. We therefore adopt the detectability criteria defined in (Collett 2015) and only use the detectable lenses to form our training set.

We modified LENSPOP to generate mock images with appropriate seeing (0.8" in all bands) and shot noise for the CFHTLS, but without readnoise or shot noise from the sky background. These mock images were then superimposed on backgrounds chosen randomly from a tile of the CFHTLS survey. Non lenses were generated in the same way but with the source fluxes set to zero; this results in images with synthetic early-type galaxies drawn from the same distribution as our lenses but with no source light.

The redshift distributions of the simulated lenses and sources are as per Collett (2015) and SWII.

For the whole-survey search, where every pixel of the image database was tested, the ConvNets are required to distinguish strong lensing systems from any other object visible in the survey sky. In the case of the first training set, negative examples consist of images centered on an assortment of galaxies (ellipticals, spirals and irregulars) with no lensed source (Figure 1). For the second training set, negative examples containing empty sky, spiral galaxies, stars, and artifacts, drawn from a random position on a survey tile as 60x60 pixel stamps from the survey imaging, are used. The two training sets (TS1 and TS2) are outlined in Table 4. 20% of the images in each training set are excluded from training and set aside as validation sets for measuring accuracy during the training process.

For the catalog-based search, all tested images are postage stamps of pre-selected red elliptical galaxies and so the training sets are constructed accordingly. Two further training sets are constructed. The first (TS3) uses SIMCT simulated lenses with a small random translation of 0-10 pixels. The negative training set consists of an equal number of ETGs randomly selected from our catalog.

<sup>5</sup> <https://github.com/anupreeta27/SIMCT>

<sup>6</sup> <https://github.com/tcollett/LensPop>

**Table 3.** Comparison of terminology in machine learning and astronomy as applied to sets of candidate objects.

Astronomical term	Machine learning term
<b>Purity:</b> The fraction of the returned sample that consists of genuine examples of the objects studied.	<b>Precision:</b> The fraction of the examples identified by the machine learning algorithm that are true positives. $\frac{TP}{TP+FP}$
<b>Completeness:</b> The fraction of the genuine objects studied that are included in the returned sample.	<b>Recall:</b> The fraction of the positive examples identified by the machine learning algorithm ( <b>True Positive Rate</b> ): $\frac{TP}{TP+FN}$
	<b>False Positive Rate:</b> The fraction of negative examples classified incorrectly by the machine learning algorithm: $\frac{FP}{FP+TN}$
	<b>Accuracy:</b> The fraction of examples classified correctly by the machine learning algorithm: $\frac{TP+TN}{total\ size}$

**Table 4.** Summary of the image sets used to train the corresponding convolutional neural networks. SIMCT simulations use real survey ETGs and simulated sources; LensPop simulates both source and deflector.

Training set	Simulations	Pos examples	Neg examples	Total
TS1	SIMCT	6657	7813	14470
TS2	LENSPOP	11799	12910	24709
TS3	SIMCT	3950	3950	7900
TS4	LENSPOP	40000	40000	80000

The second (TS4) consists of 40,000 LENSPOP-simulated lenses, again with up to 10-pixel scatter from the centre of the image, and an equal number of catalog ETGs as the negative training set (unlike TS2, which included stars, empty sky, etc. in the negative set). The spatial jitter, added to TS3 and TS4, is introduced in order to prevent the ConvNets from developing an over-sensitivity to position in the image.

Determining the optimal size of a training set is not straight forward, as it depends on the number of weights to be trained and the complexity of the features the network must learn. Large-scale visual recognition applications typically require training sets in the millions. We assume that, given the small number of convolutional layers (as outlined below) and classes (two) that a training set of order a few times  $10^4$  to  $10^5$  examples will suffice to train our networks.

### 3.2 Network Architecture and Pipeline

The convolutional neural networks were trained using the Berkeley Caffe deep learning package (Jia et al. 2014). Two network architectures are used, the first (ARCH1) consisting of two convolutional layers and two fully connected layers of 4096 neurons each, the second (ARCH2) consisting of three convolutional layers and two fully-connected layers of 1024 neurons each (Figure 2). These networks with two to three convolutional layers can be compared to the five of the ILSVRC Alexnet (Krizhevsky et al. 2012) and up to hundreds in the more recent literature (Simonyan & Zisserman 2014). A smaller network requires less time to train, and our architecture is justified by the smaller and morphologically simpler dataset as well as the low number of categories - two - compared to more general computer vision applications (c.f. ILSVRC,  $10^6$  images, 1000 categories). ARCH2 added a convolutional layer and reduced the number of fully connected neurons; this design resulted in a smaller number of weights to train ( $1.1 \times 10^6$ , versus  $1.8 \times 10^7$  in ARCH1). Between each layer we use a rectified linear unit ("ReLU") activation function (Nair & Hinton 2010),  $y = \max(0, x)$ .

The output of each ConvNet was a softmax layer<sup>7</sup> resulting in a real-valued number  $0 \leq s \leq 1$  which we interpret as the network's confidence that the candidate image is a lens.

The networks are trained with input images of dimension 60x60 pixels in three colours. These dimensions are chosen as, in the case of CFHTLS imaging at .186" per pixel, this is large enough to contain the test set lenses and small enough to prove highly performant in training and searching. The FITS *irg* images are converted to RGB images scaled with an arcsinh stretch using HUMVI (Marshall et al. 2015) and supplied to the ConvNet as vectors of 10800 (60x60x3) floating-point numbers. Training, when performed on a single NVidia K80 GPU, was typically of order a few hours for ten epochs (iterations through the entire training set). Training was conducted using stochastic gradient descent, with Nesterov momentum of 0.9 and a decaying learning rate initialised at 0.1. The network's weights were initialized according to the Xavier method (Glorot & Bengio 2010).

### 3.3 All-survey search

Two networks of the same architecture (ARCH1) are trained separately on the first two training sets outlined in Section 3.1 and Table 2. As discussed below, an ensemble of the two is used in identifying final candidate lenses. Our processing pipeline constructs the set  $C$  of candidate lenses such that for any image  $c$  with ConvNet scores  $s_1$  and  $s_2$ :

$$c \in C \text{ if } s_1(c) > t_1 \text{ and } s_2(c) > t_2 \quad (3)$$

where thresholds  $t_1$  and  $t_2$  are parameters chosen empirically to achieve an optimal balance between purity and completeness. As described below, the results presented here assume  $t_1 = t_2 = 0.95$ .

When processing each pointing image of 19354 pixels squared, our pipeline divides the image into overlapping 60x60 cutouts (in three colours) advanced with a 10-pixel stride, so that any given point in the field will be tested at different positions in 36 cutouts. This means that for each square degree of sky in the survey, 3.7 million overlapping images are tested with each of the two trained ConvNets.

We filter the candidates that meet this criterion further by removing those that are not robust under small translations. We find that rejecting candidates that occurred in isolation, with no neighbouring candidates in overlapping images, reduced the false positive rate.

<sup>7</sup> A normalised exponential function that squashes an array of  $N$  real values to a  $N$ -dimensional vector  $\mathbf{v}$  such that  $0 < v_i < 1$  and  $\sum(v_i) = 1$ :  $\sigma(z)_j = \frac{e^{z_j}}{\sum_{n=1}^N e^{z_n}}$  for  $j = 1, \dots, n$ .

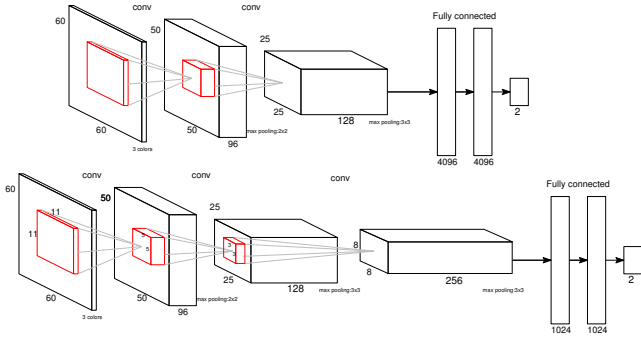


**Figure 2.** Convolutional network architectures. The networks consist of a) two convolutional layers with kernel sizes 11x11 and 5x5, with 96 and 128 feature maps respectively (ARCH1); and b) three convolutional layers with kernel sizes 11x11, 5x5 and 3x3 with 96, 128 and 256 feature maps (ARCH2). Between each layer is a ReLu activation layer and dropout of 0.5 is applied before each fully connected layer.

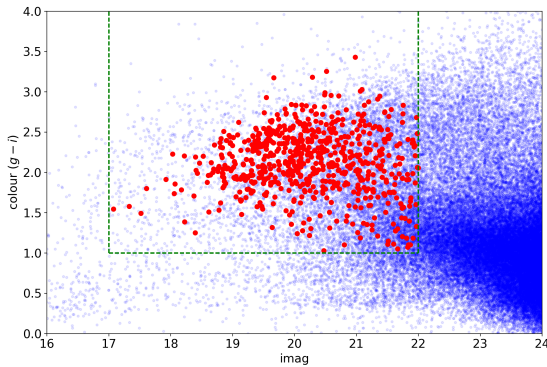


**Figure 3.** Colours and magnitude of sources from the CFHTLS photometric catalog (blue) and sources corresponding to lensing systems and promising candidates reported in the literature (red). Our search considers only sources within the box marked in green, where ( $17 < \text{mag}_i < 22$ ) and ( $g - i > 1$ ) representing 1.4 million of the 36 million catalogued sources.

### 3.4 Catalog-based search

For the catalog-based search, we restrict the search to catalogued sources in a subset of colour-magnitude space consistent with likely lensing galaxies. We expect massive ETGs to be the best candidate deflectors due to their higher lensing potential, and so select sources that are both bright ( $17 < \text{mag}_i < 22$ ) and red ( $g - i > 1$ ). These thresholds are confirmed by examining the position in colour-magnitude space of known lensing systems and candidates within the CFHTLS footprint (see Figure 3) according to the 3" aperture photometry available in the survey catalog. 98% of these lenses are within the cut, which contains 5.6% of the 36 million catalogued sources. We apply these cuts to the CFHTLS catalog, excluding those sources flagged as stars, to build our catalog of 1,402,222 sources.

For each source in the catalog, 60x60 pixel postage stamps centered on the source are created and scored by each of the four ConvNets.

## 4 RESULTS

### 4.1 Simulated Lenses

All of the networks trained were able to distinguish simulated lenses from non-lenses with high accuracy. On test sets not used for training, containing equal numbers of simulated lenses and non-lenses, the four networks trained were able to achieve accuracy of 98.4%, 91.6%, 99.2%, and 99.8%, respectively. This performance is depicted in Figure 4. On test sets of 2000 simulated lenses, the four networks achieved both high purity (94%, 94%, 100%, 100%) and completeness (96%, 95%, 99%, 100%) with a score threshold of 0.5.

The networks' performance dropped when applied to simulated lenses generated by the method not used for training, indicating a preference for the peculiarities of each particular simulation method. Figure 4 depicts the degraded performance for networks 3 and 4 on each other's test sets. However, both the mean and maximum scores of the two networks were able to classify the combined test set with close to 100% accuracy. This fact informed the use of a combination of the two types of networks on the search of real survey images as outlined below.

### 4.2 All-survey search

Two ConvNets (ConvNet1 and ConvNet2) were trained on the training sets (described above in Section 3.1) and applied to a test set consisting of 59 512x512 pixel images centered on the lens candidates from SWII, for a combined area of 0.041 square degrees of sky ( $\sim 3900$  pixels squared), for a total of 153,459 overlapping 60x60 cutouts. The parameters  $t_1$  and  $t_2$  from Equation 3 were adjusted in order to explore the balance between true and false positives output by the system. At  $t_1 = 0.95$ ,  $t_2 = 0.95$ , after testing 153,459 images, the system recovered 25/59 of the test set's lenses and returned three false positives. These settings were used as a basis for the wider search. The candidates returned from the test set, as well as those not detected, are depicted in Figure 7.

We applied the same pipeline to 171 square degrees of the CFHTLS survey for which  $i$  or  $Y$  band,  $r$  and  $g$  band data were available. The results of the search with these parameters are summarised in Table 5. Classifying the images took approximately 100 GPU-days on NVidia K20 GPUs with 2496 cores each. After examining all of the 60x60 postage stamps with both ConvNets, 18,861 candidates were identified by the system, representing 0.1% of the survey area or about one source in 1900. Out of the 59 sources in our test set of real lens candidates, the final candidate set included 22 (37%) of them. The candidate set included a total of 63 of 565 previously reported lenses or candidates (11%), and 14 of the 103 confirmed lenses (14%). Of the remaining 18,839 candidates, the authors identified 18,400 as low quality (false positives) and 149 as potential lens candidates with grade  $> 0$ . Out of 640 million images examined, this represents a false positive rate of about 1 in 35,000. The 199 true positives represent a purity of only 1% for the estimated completeness of 11-14%.

The sample of novel candidates includes six which we rate as grade  $\geq 2$ . These candidates are included in Figure 6 and Table 6.

### 4.3 Catalog-based search

To assess the performance of the catalog-based search, we assign each known lens/candidate to the closest catalog sources. Of the



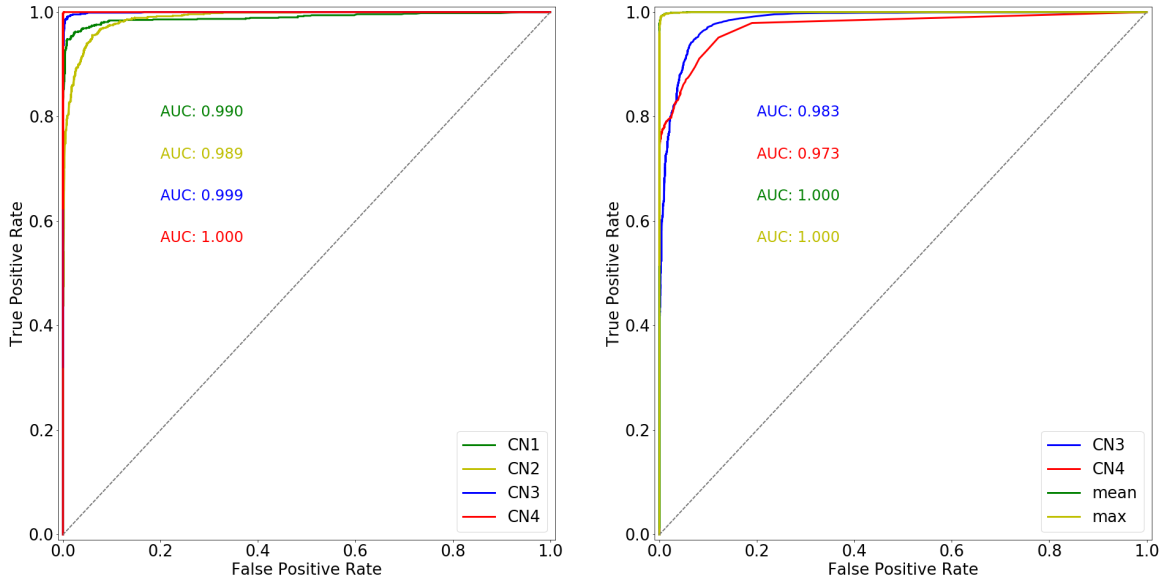


**Figure 4.** Receiver operating characteristic (ROC) curves for the trained ConvNets, depicting the trade-off between the true positive rate (recall) on the y axis, and the false positive rate (false positives/all negatives) on the x axis. Each point on the curve represents a threshold setting for the network - a lower threshold identifies more candidates (higher recall) but also more false positives (lower precision).

**Table 5.** Results of all-survey and catalog searches.

All-survey search		Catalog-based search	
Images tested	$6.4 \times 10^8$	Images tested	$1.4 \times 10^6$
Detection by either ConvNet	$2.0 \times 10^7$	Final candidate set	2,465
Detection by both ConvNets	$1.6 \times 10^5$	Fraction of images returned as candidates	$1.8 \times 10^{-3}$
Candidates robust under translation	$3.5 \times 10^4$	Test set lenses/candidates found	23/57 (40%)
Fraction of images returned as candidates	$2.9 \times 10^{-5}$	Known lenses/candidates found	117/565 (21%)
Final candidate set	18,861	Confirmed lenses found	29/104 (28%)
Test set lenses/candidates found	22/59 (37%)	New lens candidates grade > 0	266
Known lenses/candidates found	63/565 (11%)	New lens candidates grade >= 2	13
Confirmed lenses found	14/104 (13%)	False positives	2097
New candidates	199	Purity	15%
False positives	18,400	Completeness (known lenses)	21-28%
Purity	1%		
Completeness (known lenses)	11-13%		

SPACEWARPS test set lenses, two were too blue and were excluded by the colour cut leaving a test set of 57 lenses.

For the catalog-based search, each of the 1.4 million selected sources was evaluated with the ConvNets 1-4. As with the whole-survey search, the score thresholds for each ConvNet can be varied in order to assemble subsets of the tested sources to serve as candidate sets. Each subset can be assigned a true positive rate based on the number of test set lenses recovered, and a false positive rate based on the size of the set and the number of known lenses within it. The distribution of these sets in true positive-false positive space, known in machine learning literature as a receiver operating characteristic (ROC) curve, succinctly describes the trade-off between precision and recall inherent in an algorithm, and is presented in Figure 5. At one extreme, with the four threshold values of (0, 0.95, 0.95, 0.15) for the ConvNets 1-4, a candidate set of 71 candidates was produced containing 4 of the test set lenses and 10 other known lenses or candidates. With thresholds (0, 0.95, 0.55, 0), a candidate set of 2,465 sources is produced containing 23 of the test set lenses.

With a completeness of 40% with respect to the SPACEWARPS lenses, and a candidate set small enough to inspect in under an hour, this set was chosen as representative of likely practical settings and was examined by eye to evaluate overall candidate quality.

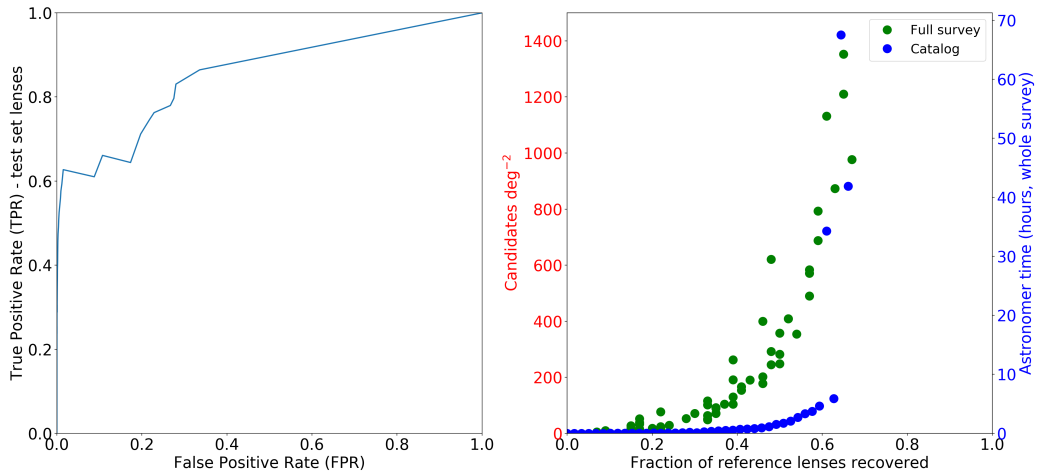
The sample contains 117 of the 565 previously known lenses, including 29/103 confirmed lenses. After visual inspection of the 2,465 candidates we identify a further 266 candidates as possible or probable lenses, including 249 possible, 15 probable and four definite lenses. The candidates with scores  $\geq 2$  are presented in Figure 6 and Table 6. 12 of the galaxies have photometric redshifts, ranging from 0.42 (CN1) to 1.13 (CN16).

Figure 7 depicts a subset of test set lenses and confirmed lenses recovered in the candidate set, and of those not recovered. There are several example of highly elliptical deflectors (potentially edge-on spirals) and redder sources amongst the missed lenses, which differ from those generated for the training set. In colour-magnitude space, there is not clear difference between the lenses found and those missed. The robot did not perform better on lenses



**Table 6.** New potential strong lenses identified in the CFHTLS wide fields by the ConvNet lensfinding robot. The 16 sources consist of the candidates identified by the algorithm that have a quality flag  $\geq 2$  and are not identified elsewhere in the literature. The i-band magnitude supplied is from CFHTLS Terapix T0007 photometric catalog 3" aperture photometry. Photometric redshifts for the deflectors are provided where available.

Candidate	search	source	RA	dec	grade	imag	$z_{phot}$
CN1	all-survey	1135_114442	32.014397	-6.962067	2.0	19.857	0.42
CN2	all-survey	1134_102957	32.773519	-7.136335	3.0	20.450	0.83
CN3	catalog	1114_035558	34.866662	-5.488730	2.5	19.18	–
CN4	all-survey	1157_073435	36.528578	-9.983405	3.0	20.323	–
CN5	catalog	1119_077854	38.123480	-6.227281	2.0	20.67	–
CN6	both	1120_144248	37.142005	-5.996789	2.0	20.68	0.84
CN7	catalog	1124_121677	33.544766	-6.093784	2.0	21.29	0.79
CN8	catalog	1133_208513	33.367565	-6.681572	3.0	20.53	0.55
CN9	both	1156_165804	37.090818	-9.645684	2.0	19.74	0.30
CN10	catalog	1163_117574	31.012133	-9.745038	2.0	21.30	0.87
CN11	catalog	1203_218233	134.733282	-1.035681	2.0	19.48	–
CN12	catalog	1309_158230	217.484603	56.535095	2.0	20.27	0.55
CN13	catalog	1314_020589	210.346656	55.951494	2.0	19.59	–
CN14	both	1328_213514	210.206937	54.738516	2.0	20.47	0.59
CN15	catalog	1403_048428	330.851737	3.811333	2.0	21.87	–
CN16	catalog	1424_168469	333.094995	-0.303149	2.0	21.71	1.13



**Figure 5.** Left: Catalog-based lensfinder true-positive/false positive response (ROC curve). 20% of the test set can be recovered with a false positive rate of .01%; 40% with a false positive rate of 0.17%; and 60% with a false positive rate of 1.17%. Right: Lensfinder recall vs. time required to inspect the produced candidate set for the whole-survey approach (green) and catalog-based search (blue). For the whole survey, 171 square degrees, we estimate 40% of findable lenses can be recovered with about 15 candidates per square degree to inspect - or one hour of inspection time for the survey.

rated as higher quality by astronomers. Of the 59 SPACEWARPS test set lenses, 30 were of grade 1-2, and 29 were of grade 2-3. Of the 2+ lenses, our system recovered 12 (41%) and of the 1s, 10 (33%).

## 5 DISCUSSION

### 5.1 Training networks on simulated images

From the results presented we conclude that convolutional neural networks trained on synthetic lenses are able to develop detectors for lensing features and identify real lenses in survey image data. Our two training sets were designed to simulate strong lenses with parameters, such as brightness and Einstein radius, similar to those lenses present in CFHTLS and discovered by the human volunteers of the SPACEWARPS project. We chose to use the SWII lenses

as a reference set since, firstly, the lenses were of a size and morphology that made finding by automated means challenging (they were not discovered in any previous CFHTLS lens search); and secondly, they allow for a comparison, in terms of efficiency of search time, with the person-hours invested in training and searching by the SPACEWARPS volunteers who discovered them. As the ConvNets are, by design, optimized to detect objects similar to the training set, our robot will not in general succeed at finding lenses that are, for instance, significantly larger in the sky, are of different colour, have point instead of extended sources (i.e. QSOs) or are not galaxy-scale lenses (i.e. clusters).<sup>8</sup>

<sup>8</sup> We have created training sets that include cluster-scale lenses and lensed QSOs, with preliminary results that indicate that these different morphologies are also learnable, but do not present that work here.

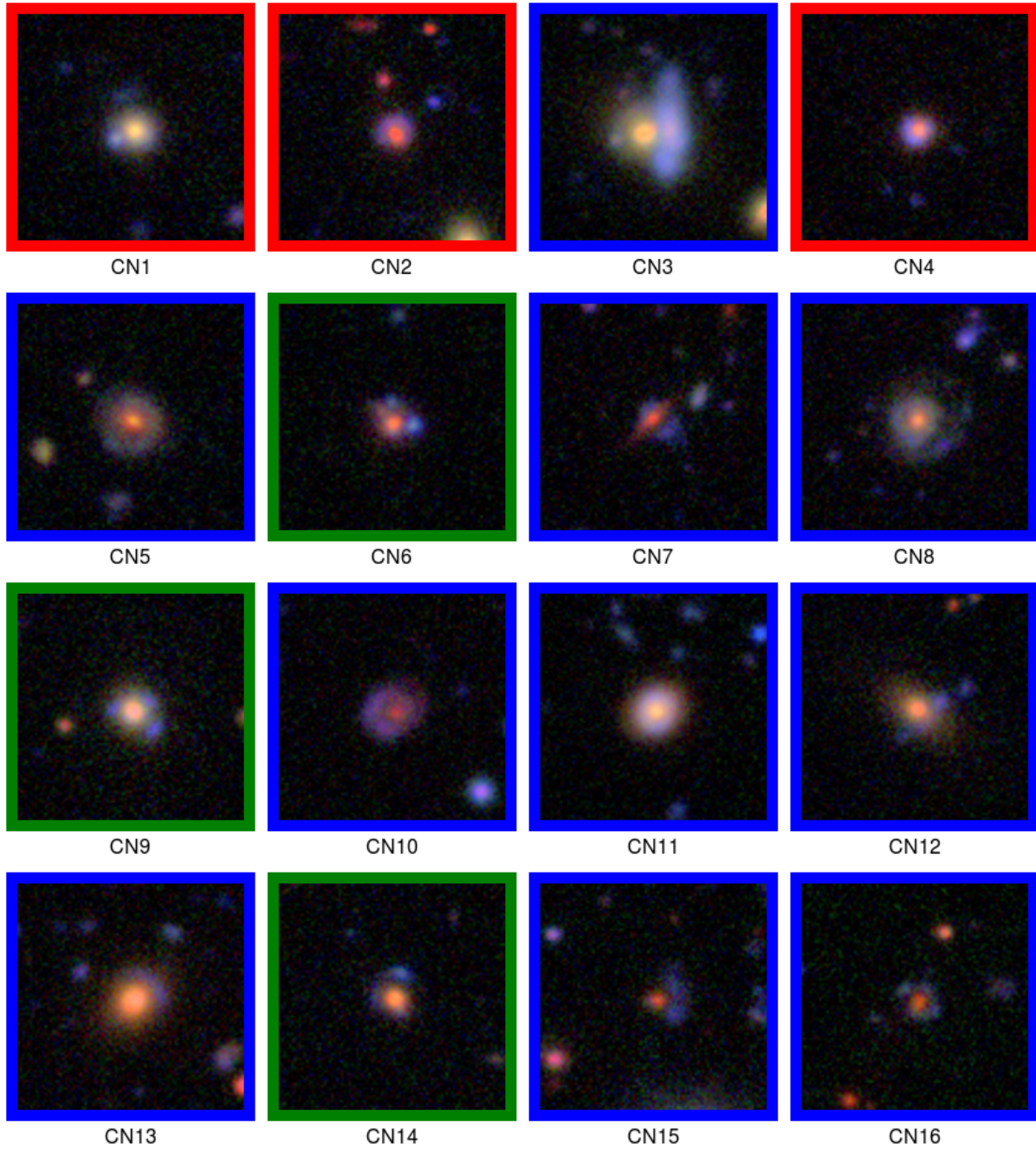


**Figure 6.** New potential galaxy-galaxy lenses detected by the ConvNet-based lens finder. *gri* composite images are shown, with the border indicating the method of discovery: red = all-survey search, blue = catalog based, green = both. The sources are described in Table 6.

Unlike a human, the ConvNets demonstrate little ability to generalise the features they have learned to situations that differ from those presented in the training set on which they were optimised. A human being might spot a lens that has the same shape as other examples but differs in colour (for instance, a red-red lens) and decide it is an unusual instance of the class; the ConvNet probably will not, as the convolutional kernels it has developed weight the contributions of the colours according to their prevalence and significance in the training set. Although there is ongoing research into classes of machine learning techniques where this weakness is addressed - for instance, Bayesian Program Learning (Lake et al.

2015), which models visual concepts as simple probabilistic programs - this is an intrinsic feature of ANNs.

A sufficiently complex ANN can be expected to learn more than just the general morphology of a gravitational lens. Any simplifications or unphysicalities in the simulations are likely to be learned by the network. Where an ANN is trained properly, the network's weights will efficiently encode the significant features of the training set. In the case of real-world images, finding such an encoding is a highly complex task, though one at which ANNs have proved highly successful. In the case of simulations, the most efficient such encoding would be the parameters of the simulation



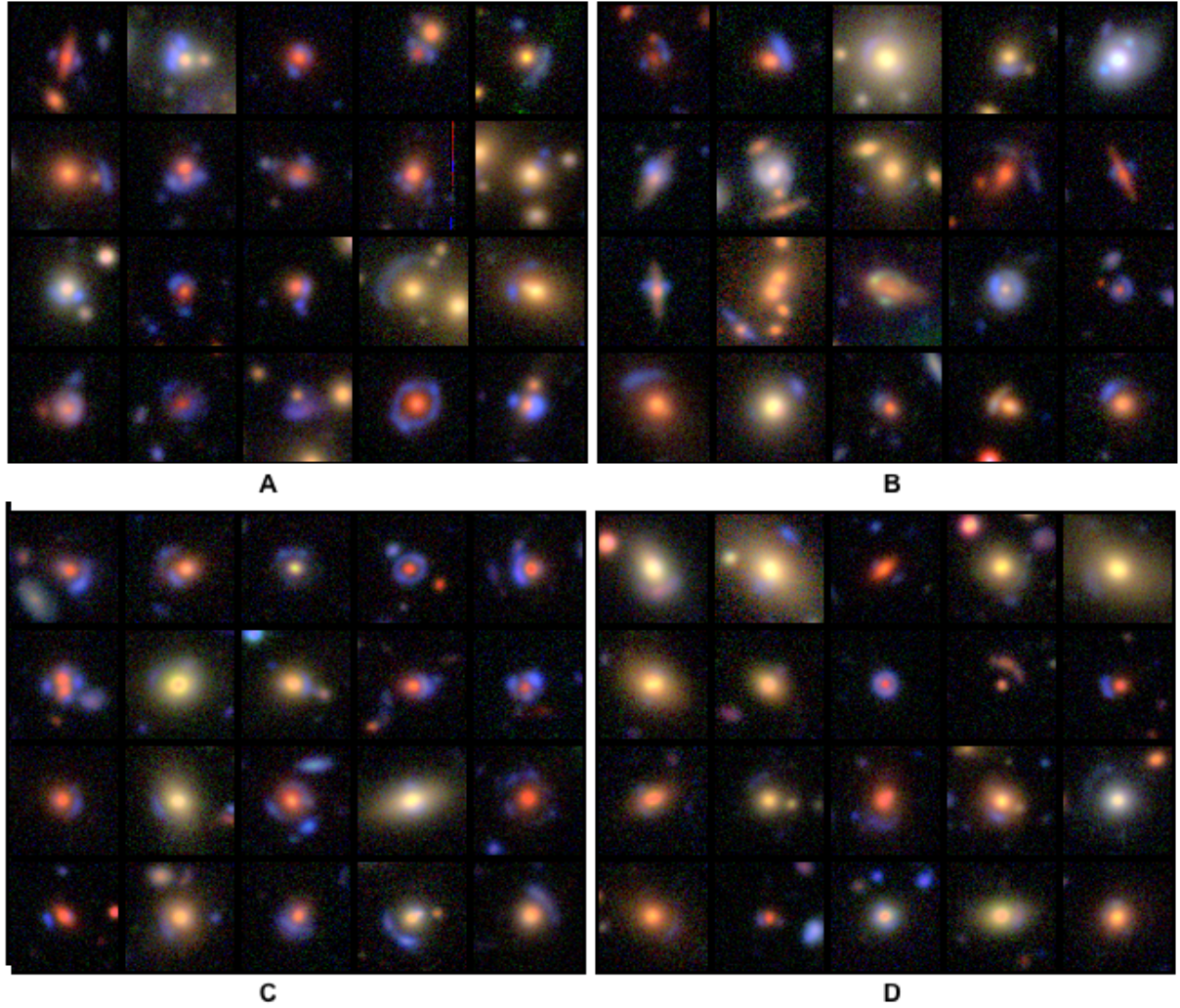


**Figure 7.** Lenses recovered by the lens finder, and those missed. Top left, A: 20 Lens candidates identified by citizen scientists of the SPACEWARPS project (More et al. 2016) recovered by the ConvNet robot in a candidate set of 2465 candidates. Top right, B: 20 SPACEWARPS lenses not recovered. Bottom left, C: 20 confirmed lenses recovered in the catalog-based search. Bottom right, D: 20 confirmed lenses not recovered. The missed SW lenses contain more cluster-scale lenses, redder sources and potential spiral deflectors; the missed confirmed lenses have fainter sources.

code itself; if an ANN is trained on a sufficiently large number of simulated images, it can be expected to become proficient at determining whether an example image could be generated by a given simulator. This type of overfitting to the training set is a hazard of using simulated training data.

In this work we deployed ConvNets with relatively simple architectures. Training much deeper networks is feasible. The motivation for deeper, more complex networks is the extraction of a richer feature set from the training data, at the expense of training time, a larger training set, and potential difficulties getting training to converge. Because of the high accuracy on simulated training, validation and test sets, we did not explore deeper networks which we deemed likely to merely overfit further to the simulations. Future work will need to explore whether deeper networks have an impact on the performance on genuine astronomical image data, especially as the simulations improve and become more complex.

## 5.2 Using an ensemble of Neural Networks

The use of ensembles of neural networks in classification or regression problems is a common practice in machine learning (Hansen & Salamon 1990; Zhou et al. 2002). According to the standard procedure, multiple networks are trained using different subsets of the training set and then (for example) averaged together to produce a final score for a given input. In complex computer vision applications this typically provides a small edge over any single network. In the case of the lensfinder, this approach is of little value as the network is already able to classify simulated training, validation and test sets with very high accuracy. The networks' performance drops when generalised to real data.

We used simulated lenses from two different sources to train our networks. Each simulation code took an approach that was physical and realistic but the resulting outputs were slightly different in appearance. By combining the two, we smooth out some of the less realistic features of each simulated set. We find that in the case of our networks, a union of two candidate sets provided good results; we only look at candidates that triggered both networks, ig-



noting those that were flagged in one network only as likely false positives. Other functions, such as a mean score or max of the two networks' scores, are also feasible approaches. Although a detailed investigation of the networks' internal activations is complex and beyond the scope of the current work, it appears that the ensemble process is effective as the networks tend to agree most often on a high score where stark lensing features are apparent, but false positives are triggered in different ways.

This approach of constructing multiple simulations and training networks separately may have application in other areas of astronomy where examples are few and simulations are required to build a training set.

We note that combining the two different sets of simulations into one and retraining the network on the combined set did not yield satisfactory results. The combined training set, with an accuracy in training of  $\sim 70\%$ , was strictly inferior to either of the separate training sets. There is no theoretical barrier to achieving similar accuracy as the ensemble with a single ConvNet of sufficient complexity, since the logic we employed of developing two sets of feature maps and weighting the outputs could be replicated within the connections of an ANN. Further experimentation with the training sets and the use of a network with additional layers and more artificial neurons is required.

### 5.3 Catalog-based versus all-survey search

Searching the entire survey - that is, feeding every pixel of the imaging data through the networks, regardless of the presence of a likely lensing galaxy - has the advantage that the maximum completeness is attainable, since no assumptions are made in selecting a subset of sources to examine. Unusual lenses of high scientific value (complex morphologies, multiple lensed sources, dark matter-dominated deflector) are more likely to be excluded by a catalog selection, and inaccurate catalog photometry may exclude others, such as the case where a bright blue source substantially shifts the color of the foreground galaxy within the photometric aperture used by the catalog source extractor. The volunteers for the SpaceWarps CFHTLS blind search were not restricted to postage stamps of ETGs but shown larger fields containing hundreds of sources, so they were freely able to nominate candidates that differed from the typical morphologies and colours used in training examples.

The disadvantages of such a wide search with automated algorithms are several. Firstly, it is computationally expensive, requiring months of GPU time for a large survey area. Secondly, lower purity in a candidate set can be expected since a much larger number of candidate images are examined (at least two orders of magnitude) per genuine lens, accumulating more false positives. Finally, unless the training set explicitly includes unusual examples (such as a lens with no visible deflector) they are unlikely to be detected in any case by the networks.

Restricting the search for strong lenses to preselected potential deflector galaxies simplifies the search in several ways. Firstly, it reduces the search area enormously, and presents a much purer (though inevitably less complete) set of images to the network. Secondly, a catalog-based search simplifies the generation of a training set. Both the positive and negative training images can all be centered on a bright elliptical galaxy, since all future candidate images will follow the same convention.

The catalog-based search was significantly more efficient in recovering known lenses by producing candidate sets of considerably higher purity (precision) for a particular completeness (recall) value as measured against known lenses in the sample. Although

the networks trained for the whole-survey search had a lower false positive rate of 1 in 35,000 versus 1 in 671 for the catalog-based search, this can be explained by the relative ease of distinguishing galaxy-galaxy lenses from empty sky, spiral galaxies, stars and other unlikely candidates.

Of the 63(14) known(confirmed) lens candidates detected in the all-survey search, 44(11) of them were included in the catalog sample. Of the six novel candidates we rate as grade  $\geq 2$  in the all-survey search, three of them were also detected in the catalog-based search.

### 5.4 Quantifying the performance of the robot

The outputs of the ConvNets are real numbers  $\in (0, 1)$  which we interpret as a measure of confidence or of candidate quality. The minimum confidence level for which we include candidates in our output set is a free parameter in this range. Depending on the values chosen, the ConvNets are able to produce a set of candidate images of almost arbitrary size but with highly variable purity and completeness. In practical terms this means that, depending on the particular application, the robot can produce larger or smaller candidate sets by making trade-offs in the purity and completeness.

Analysis of the performance of a lens-finding robot is complicated by several factors. Performance is optimal when it finds all potential lenses (lens quality  $> 0$ ) and no false positives (quality  $= 0$ ). Performance degrades both as the number of false positives increases and the fraction of true positives recovered decreases. We can fully populate the confusion matrix (Table 7) for our system as applied to training, validation and test sets of simulated lenses. Similarly, we can measure performance against the test set of SPACEWARPS candidates, since the lens candidates are all known (see Table 8).

It is the robot's performance on real imaging data is of most interest. On the wider search, quantifying the performance is more complicated, as candidates which are not previously reported as lenses in other searches may not be considered false positives if they are sufficiently interesting. Similarly, we do not know how many lenses remain undetected in the survey and so the false negative rate is likewise uncertain. With this caveat in mind, we use the data from the test set, combined with more approximate metrics gained from the wider search in our consideration of our robot's performance on the CFHTLS sky.

By varying the free parameters  $t_1$  and  $t_2$  (Equation 3) we can more fully explore the balance between precision and recall afforded by our robot. For any point in the  $(t_1, t_2)$  space we can plot the rate of true positives (recall) and false positives (False Positives/Condition Negatives) to produce a Receiver Operating Characteristic (ROC) curve (Fawcett 2004) as presented in Figure 4 and Figure 5. The ideal curve includes the point  $(x = 0, y = 1)$  where all positive examples are detected with no false positives, and has an area under the curve (AUC) of 1. The worst case scenario, where the robot guesses randomly, lies on the line  $y = x$ .

To construct a confusion matrix and estimate purity and completeness (precision and recall) on the real survey imaging data, we use the 565 previously reported lens candidates as an approximation of the complete sample if findable lenses in the survey.

To estimate purity, we also consider interesting novel candidates. Any candidate to which we assign a grade  $> 0$  after visual inspection we consider a true positive; other candidates we count as false positives. Of our final candidate set of 2465 lenses, 117 had been previously identified as potential lenses, including 23/57 (40%) SPACEWARPS lenses and 29/103 (28%) confirmed lenses. The

	Condition Positive (CP)	Condition Negative (CN)
Test positive	True Positives (TP)	False Positives (FP)
Test negative	False Negatives (FN)	True Negatives (TN)

**Table 7.** Template for the confusion matrix of a classification algorithm.

authors agreed that 364 candidates were of grade 1 or greater, including 98 of the 117 reported lenses in the sample; 526 images were graded with score  $> 0$  by at least one reviewer, including 102 previously known lenses, meaning that between 379 and 537 of the sample were interesting candidates. Thus when applied to CFHTLS data, our robot produced a sample with a purity of between 15-22%. The 117 of 565 known lenses (22%) returned in our sample, including 28% of confirmed lenses, gives us an estimate of completeness with respect to the highest quality detectable lenses.

Our sample included at most 2086 false positives from a set of 1.4 million true negatives tested, for a false positive rate of 0.15%, or one in 671.

Although we included all the known lenses and candidates previously discovered in CFHTLS image searches in our analysis above, a significant number of them are cluster-scale lenses, have non-elliptical deflectors or red sources, or are extremely faint according to a subjective ranking by the authors. These differ significantly from the examples simulated in the training sets we generated. We estimate approximately 15% of the sample, both confirmed and unconfirmed, meet one or more of these conditions. Excluding these from the known lenses, our lens finder recovered 25% of previously reported and 33% of confirmed lenses; this may better approximate the performance of a robot engineered specifically for lenses of a particular morphological class, i.e. galaxy-galaxy lenses, and give some indication of gains that might be realised with a training set that includes greater morphological diversity.

### 5.5 Context and practice

The ConvNets were more prone to identify clear false positives than a professional astronomer or even a human volunteer with minimal training; for instance, across the whole survey each ConvNet identified of order  $10^7$  candidates with confidence  $> 0.5$ , amounting to a few percent of images tested. A key challenge was how to best use the classification data to minimise false positives, i.e. candidates we judge very unlikely to be lensing systems. Intrinsic to the lens-finding problem is the rarity of lenses on the sky. If we expect approximately one lens per square degree of sky (as per Treu 2010), then in an all-survey search of the scale we conducted, a false positive rate of only 1 in 1000 would mean that quality lens candidates would be outnumbered by false positives at a ratio of about 4000:1.

An alternate way to examine the trade-off between precision and recall is presented in Figure 5, which plots the fraction of lenses recovered in the candidate set against the average size of the candidate set per square degree of sky. Assuming an astronomer could search these candidates for quality lenses at a rate of 60 per minute<sup>9</sup>, the amount of time required to process the whole survey's candidates is indicated on the right. For a whole-survey

<sup>9</sup> When presented as 10x10 montages containing 0 to a few quality candidates, we found this rate to be feasible.

	Actual positive	Actual negative
Test positive	25	3
Test negative	34	153,459

**Table 8.** Confusion matrix for the all-survey test set containing 153,000 images including 59 SPACEWARPS lens candidates. The candidate set is produced by taking all candidates where the two ConvNets give a score  $s > 0.95$ .

search, to recover 50% of lenses one would need to examine approximately 250 candidates per square degree, 0.2% of the field's area. To recover a minimum of one high-quality candidate, examining a candidate set of a few hundred postage stamps for the whole survey would be required. The catalog-based search is more efficient, with 50% recall achievable with only 40 candidates per square degree. By restricting candidate sources even further, to  $19.5 < \text{mag}_i < 20.5$  and  $1.8 < g - i < 2.5$ , and setting the thresholds aggressively we were able to generate small, pure but highly incomplete candidate sets, for instance a set containing only 7 candidates for the entire survey but including 4 known lenses (a purity of 57%). The lensfinder can be used to quickly find some of the best quality lenses, but astronomer time required grows quickly as desired completeness increases (see Section 4.3 and Figure 8).

## 6 CONCLUSIONS

We present an application of convolutional neural networks to the automated identification of potential strong lenses. Deep learning techniques have advanced computer vision in many other fields and have already found many promising applications in astronomy. Our work demonstrates that a ConvNet can extract morphological and colour-space features from examples of strong lenses, and also that the use of simulations in training sets can be used to train a lens-finding robot to be of practical use on real astronomical data. For a survey covering 170 degrees to an r-band depth  $\sim 24.83$  we were able to generate a candidate set that was 28% complete in terms of confirmed, findable lenses; 15% pure with respect to possible lenses; and could be visually inspected by a human in under an hour. This performance, yielding  $\sim 14$  candidates per square degree, is comparable in sample size to other automated methods such as RINGFINDER Gavazzi et al. (2014). The ConvNet-based method allows for higher completeness at the cost of decreasing purity.

Using the pipeline developed here we find that a ConvNet-based lensfinder, under the conditions of the CFHTLS and using a catalog-based search with optimised settings, could produce a candidate set that yielded of order one good quality lens candidate per square degree of survey sky with an investment of astronomer inspection time of under half a minute each. We are optimistic that this rate of discovery can be replicated or exceeded in other extant and future image surveys. This compares favourably to previous robotic searches and has the potential to greatly increase the efficiency of future lens searches, especially as the algorithm is refined.

CFHTLS was chosen as a yardstick to evaluate ConvNet performance as it has been extensively searched for lenses using other methodologies. Given the performance we obtained, this method would appear to be a promising way to explore new fields. Using synthetic training sets generated with parameters matching other current and upcoming surveys such as DES and LSST, the convnets can be retrained and readily applied to another data pipeline. As well as generating candidate sets from these surveys, this method



**Figure 8.** An example of a candidate set with high purity (50%) but low completeness (1.4%). By restricting the search to sources with  $19.5 < \text{mag}_i < 20.5$  and  $1.8 < g - i < 2.5$ , and setting the ConvNet thresholds such that only a small candidate set is returned, we produced this set of 16 candidates including eight previously known lenses (left).

could also be used to produce candidates for revision by citizen scientists, complementing efforts like SPACEWARPS by screening candidates but relying on human volunteers and the SPACEWARPS quality algorithm to purify the sample before review by astronomers.

Given the demonstrated effectiveness of convolutional neural networks in computer vision applications such as classification and detection of everyday objects, it has proven to be a safe assumption that, if there is enough information in an image for a human expert to extract meaning, a properly-designed ConvNet is likely to also converge on a suitable feature extraction strategy. The SPACEWARPS project, by providing rapid training to human volunteers, demonstrated that enough information is present in images of galaxies under the conditions of CFHTLS resolution and seeing.

Further work includes refining the training sets to reduce false positives and to better detect lenses with a wider range of morphologies, including lensed QSOs and cluster-scale lenses; testing an increase in the size of the training sets and the number of convolutional layers in the network; and retraining the networks with good candidates and false positives identified in visual inspection. Exploring the ensemble approach further, for instance with training sets composed of simulated lenses in discrete bins of source magnification and Einstein radius, may aid in developing a detector capable of discriminating the brightest and most promising lenses more efficiently.

Convolutional neural networks have also recently been employed for lens finding in the Kilo-Degree Survey (KiDS) (Petrillo et al. 2017) and simulations of LSST (Lanusse et al. 2017). The differences in survey data quality and the types of lens targeted make a direct comparison difficult. However, our method of using multiple training sets and ConvNets appears to give more probable lens candidates per square degree than the Petrillo et al ConvNets, although at the cost of a factor four more human classification time. This lower purity is unlikely to be a relative deficiency of our method; we targeted smaller Einstein radius lenses where seeing makes the classification problem much harder.

## References

Alard C., 2006, arXiv:astro-ph/0606757  
 Amiaux J., et al., 2012, arXiv:1209.2228 [astro-ph] 10.1117/12.926513, p. 84420Z  
 Auger M. W., Treu T., Bolton A. S., Gavazzi R., Koopmans L. V. E., Marshall P. J., Moustakas L. A., S. Burles 2010, *ApJ*, 724, 511  
 Blandford R. D., Narayan R., 1992, *ARA&A*, 30, 311

Bom C. R., Makler M., Albuquerque M. P., Brandt C. H., 2017, *A&A*, 597, A135  
 Bonvin V., et al., 2016, *MNRAS*, p. stw3006  
 Bottou L., 2010, in Lechevallier Y., Saporta G., eds., Proceedings of COMPSTAT'2010. Physica-Verlag HD, pp 177–186, doi:10.1007/978-3-7908-2604-3\_16  
 Bradač M., Schneider P., Steinmetz M., Lombardi M., King L. J., Porcas R., 2002, *A&A*, 388, 373  
 Brault F., Gavazzi R., 2015, *A&A*, 577, A85  
 Cabanac R. A., et al., 2007, *A&A*, 461, 813  
 Cao Z., Qin T., Liu T.-Y., Tsai M.-F., Li H., 2007, in Proceedings of the 24th International Conference on Machine Learning. ICML '07. ACM, New York, NY, USA, pp 129–136, doi:10.1145/1273496.1273513  
 Chan J. H. H., Suyu S. H., Chiueh T., More A., Marshall P. J., Coupon J., Oguri M., Price P., 2015, *ApJ*, 807  
 Choi Y.-Y., Park C., Vogeley M. S., 2007, *ApJ*, 658, 884  
 Collett T. E., 2015, *ApJ*, 811, 20  
 Collett T. E., Auger M. W., 2014, *MNRAS*, 443, 969  
 Collett T. E., et al., 2017, arXiv:1703.08410 [astro-ph]  
 Connolly A. J., et al., 2010, in Proc. SPIE. pp 77381O–77381O–10, doi:10.1117/12.857819  
 Dieleman S., Willett K. W., Dambre J., 2015, *MNRAS*, 450, 1441  
 Duchi J., Hazan E., Singer Y., 2011, *J. Mach. Learn. Res.*, 12, 2121  
 Einstein A., 1936, *Science*, 84, 506  
 Elyiv A., Melnyk O., Finet F., Pospieszalska-Surdej A., Chiappetti L., Pierre M., Sadibekova T., Surdej J., 2013, *MNRAS*, 434, 3305  
 Estrada J., et al., 2007, *ApJ*, 660, 1176  
 Fawcett T., 2004, *Mach. Learn.*, 31, 1  
 Fukushima K., 1980, *Biol. Cybernetics*, 36, 193  
 Gavazzi R., Marshall P. J., Treu T., Sonnenfeld A., 2014, *ApJ*, 785, 144  
 Glorot X., Bengio Y., 2010, in International Conference on Artificial Intelligence and Statistics. pp 249–256  
 Goodfellow I., Pouget-Abadie J., Mirza M., Xu B., Warde-Farley D., Ozair S., Courville A., Bengio Y., 2014, in Ghahramani Z., Welling M., Cortes C., Lawrence N. D., Weinberger K. Q., eds., Advances in Neural Information Processing Systems 27. Curran Associates, Inc., pp 2672–2680  
 Hansen L. K., Salamon P., 1990, *IEEE Trans. Pattern Anal. Mach. Intell.*, 12, 993  
 He K., Zhang X., Ren S., Sun J., 2015, ArXiv Prepr. ArXiv151203385  
 Hecht-Nielsen R., 1989, in , International Joint Conference on Neural Networks, 1989. IJCNN. pp 593–605 vol.1, doi:10.1109/IJCNN.1989.118638  
 Hinton G. E., Salakhutdinov R. R., 2006, *Science*, 313, 504  
 Hinton G. E., Srivastava N., Krizhevsky A., Sutskever I., Salakhutdinov R. R., 2012, arXiv:1207.0580 [cs]  
 Hoyle B., 2016, *Astron. Comput.*, 16, 34  
 Huertas-Company M., et al., 2015, *ApJS*, 221, 8  
 Hyde J. B., Bernardi M., 2009, *MNRAS*, 396, 1171  
 Ivezić Z., et al., 2008, arXiv:0805.2366 [astro-ph]



- Jia Y., Shelhamer E., Donahue J., Karayev S., Long J., Girshick R., Guadarrama S., Darrell T., 2014, arXiv:1408.5093 [cs]
- Jordan M., Mitchell T., 2015, *Science*, p. 255
- Joseph R., et al., 2014, *A&A*, 566, A63
- Keeton C. R., 2001, arXiv:astro-ph/0102340
- Krizhevsky A., Sutskever I., Hinton G. E., 2012, in Pereira F., Burges C. J. C., Bottou L., Weinberger K. Q., eds., , *Advances in Neural Information Processing Systems 25*. Curran Associates, Inc., pp 1097–1105
- Lake B. M., Salakhutdinov R., Tenenbaum J. B., 2015, *Science*, 350, 1332
- Lanusse F., Ma Q., Li N., Collett T. E., Li C.-L., Ravanbakhsh S., Mandelbaum R., Poczós B., 2017, preprint, 1703, arXiv:1703.02642
- LeCun Y., Boser B., Denker J. S., Henderson D., Howard R. E., Hubbard W., Jackel L. D., 1989, *Neural Comput.*, 1, 541
- Lecun Y., Bottou L., Bengio Y., Haffner P., 1998, *Proc. IEEE*, 86, 2278
- Lenzen F., Schindler S., Scherzer O., 2004, *A&A*, 416, 11
- Marshall P. J., Hogg D. W., Moustakas L. A., Fassnacht C. D., Bradač M., Tim Schrabback Blandford R. D., 2009, *ApJ*, 694, 924
- Marshall P., Sandford C., More A., More B., More H., 2015, *Astrophysics Source Code Library*, p. ascl:1511.014
- Marshall P. J., et al., 2016, *MNRAS*, 455
- More A., Cabanac R., More S., Alard C., Limousin M., Kneib J.-P., Gavazzi R., Motta V., 2012, *ApJ*, 749, 38
- More A., et al., 2016, *MNRAS*, 455
- Nair V., Hinton G. E., 2010, in *Proceedings of the 27th International Conference on Machine Learning (ICML-10)*. pp 807–814
- Newton E. R., Marshall P. J., Treu T., Auger M. W., Gavazzi R., Bolton A. S., Koopmans L. V. E., Moustakas L. A., 2011, *ApJ*, 734
- Oguri M., Marshall P. J., 2010, *MNRAS*, 405, 2579
- Oguri M., et al., 2012, *AJ*, 143, 120
- Oguri M., Rusu C. E., Falco E. E., 2014, *MNRAS*, 439
- Ostrovski F., et al., 2017, *MNRAS*, 465
- Petrillo C. E., et al., 2017, arXiv:1702.07675 [astro-ph]
- Quider A. M., Pettini M., Shapley A. E., Steidel C. C., 2009, *MNRAS*, 398
- Refsdal S., 1964, *MNRAS*, 128, 307
- Rosenblatt F., 1957, Cornell Aeronaut. Lab
- Russakovsky O., et al., 2015, *Int J Comput Vis*, 115, 211
- Schawinski K., Zhang C., Zhang H., Fowler L., Santhanam G. K., 2017, arXiv:1702.00403 [astro-ph, stat]
- Schneider P., Kochanek C., Wambsganss J., 2006, *Gravitational Lensing: Strong, Weak and Micro*. Saas-Fee Advanced Courses Vol. 33, Springer Berlin Heidelberg, Berlin, Heidelberg, doi:10.1007/978-3-540-30310-7
- Seidel G., Bartelmann M., 2007, *A&A*, 472, 12
- Simonyan K., Zisserman A., 2014, arXiv:1409.1556 [cs]
- Sonnenfeld A., Treu T., Gavazzi R., Suyu S. H., Marshall P. J., Auger M. W., Nipoti C., 2013, *ApJ*, 777, 98
- Sonnenfeld A., Treu T., Marshall P. J., Suyu S. H., Gavazzi R., Auger M. W., Nipoti C., 2015, *ApJ*, 800
- Suyu S. H., et al., 2013, *ApJ*, 766
- Syget J. F., Tu H., Fort B., Gavazzi R., 2010, *A&A*, 517, A25
- Szegedy C., Reed S., Erhan D., Anguelov D., 2014, *ArXiv Prepr. ArXiv14121441*
- Tewes M., et al., 2013, *A&A*, 556
- Thanjavur K. G., 2009, PhD Thesis. University of Victoria, Canada
- The DES Collaboration 2005, arXiv:astro-ph/0510346
- Treu T., 2010, *ARA&A*, 48, 87
- Treu T., Ellis R. S., 2015, *Contemp. Phys.*, 56, 17
- Treu T., Koopmans L. V. E., 2002, *ApJ*, 575, 87
- Treu T., Koopmans L. V. E., 2004, *ApJ*, 611, 739
- Walsh D., Carswell R. F., Weymann R. J., 1979, *Nature*, 279, 381
- Wambsganss J., 1998, *Living Reviews in Relativity*, 1, 12
- Zeiler M. D., 2012, arXiv:1212.5701 [cs]
- Zeiler M. D., Fergus R., 2014, in Fleet D., Pajdla T., Schiele B., Tuytelaars T., eds., , Vol. 8689, *Computer Vision – ECCV 2014*. Springer International Publishing, Cham, pp 818–833
- Zheng W., et al., 2012, *Nature*, 489, 406
- Zhou Z.-H., Wu J., Tang W., 2002, *Artificial Intelligence*, 137, 239
- Zwicky F., 1937, *Phys. Rev.*, 51, 290